Journal of Molecular Spectroscopy 332 (2017) 86–93

Contents lists available at ScienceDirect

Journal of Molecular Spectroscopy

journal homepage: www.elsevier.com/locate/jms

Photodetachment spectroscopy and resonant photoelectron imaging of cryogenically-cooled deprotonated 2-hydroxypyrimidine anions

Dao-Ling Huang [1], Guo-Zhu Zhu [1], Yuan Liu, Lai-Sheng Wang *

Department of Chemistry, Brown University, Providence, RI 02912, USA

ARTICLE INFO

Article history:
Received 12 September 2016
In revised form 28 October 2016
Accepted 31 October 2016
Available online 5 November 2016

Keywords:
Dipole-bound state
Photodetachment spectroscopy
Vibrational autodetachment
Resonant photoelectron imaging

ABSTRACT

We report a photodetachment and high-resolution photoelectron imaging study of cold deprotonated 2-hydroxypyrimidine anions, $C_4H_3N_2O^-$. Photodetachment spectroscopy reveals an excited dipole-bound state (DBS) of $C_4H_3N_2O^-$ with a binding energy of 598 ± 5 cm^{-1} below the detachment threshold of 26,010 ± 5 cm^{-1}. Twenty vibrational levels of the DBS are observed as resonances in the photodetachment spectrum, with three below the detachment threshold and seventeen above the threshold. By tuning the detachment laser to the above-threshold vibrational resonances, highly non-Franck-Condon photoelectron spectra are obtained. Nine fundamental vibrational frequencies are resolved, including six symmetry-forbidden modes. The 598 cm^{-1} binding energy for the DBS is quite high due to the large dipole moment of the $C_4H_3N_2O^{\cdot}$ radical (>6 D). However, no evidence of a second DBS is observed below the detachment threshold.

1. Introduction

Neutral molecules possessing large dipole moments can bind an excess electron in a diffuse orbital to form dipole-bound anions [1,2]. Fermi and Teller [3] first predicted a minimum dipole moment of 1.625 D for a point dipole to bind an electron. Subsequent studies by considering the rotational effects in real molecules increased the critical dipole moment up to 2.0 D [4–6]. A more realistic estimate of 2.5 D is commonly accepted, according to practical experimental observations [7,8]. Ground-state dipole-bound anions have been produced via Rydberg electron transfer [7–10] and low-kinetic-energy electron attachment under supersonic expansion [11–13], and their weakly-bound nature has been confirmed by field detachment [7–10] and photoelectron spectroscopy (PES) [11–13]. Valence-bound anions with dipolar neutral cores can support dipole-bound states (DBS's) just below the electron detachment threshold as excited states of the anions, which have been observed as resonances in photodetachment cross sections [14–18] and investigated via high-resolution photodetachment spectroscopy [16–18]. Dipole-bound states have been suggested to act as a "doorway" to the formation of valence-bound anions [19–21]. Excited DBS's have also been observed in solvated I^- as charge transfer to solvent states [22–24]. Interestingly, DBS's have also been postulated as potential carriers of the diffuse interstellar bands in astrophysics [25–27].

Autodetachment from selected vibrational levels of an excited DBS was first observed in cryogenically-cooled phenoxide anions [28]. Mode-specific autodetachment was observed, leading to highly non-Franck-Condon resonant PE spectra, due to the $\Delta v = -1$ propensity rule [29,30]. DBS's as near-threshold excited states have been observed in a number of cryogenically-cooled anions [31–35] and used to obtain resonant PES. Violation of the $\Delta v = -1$ propensity rule has been observed, particularly for low-frequency vibrational modes, due to anharmonic effects. It has been shown that resonant PES via autodetachment of selected vibrational levels of the DBS can yield much more vibrational information, in particular for low-frequency and Franck-Condon-inactive vibrational modes [31–34]. Because different conformers of a dipolar molecular radical have different dipole moments, we have shown that conformation-selective resonant PES via DBS is possible [35].

Molecules with sufficiently large dipole moments may possess more than one bound DBS. Early studies of a fixed dipolar system concluded that 9.64 D is required for the second DBS (π-type) [36,37]. Considering the rotational effects, Garrett predicted a critical dipole moment of 4.5 D for the second DBS [38,39]. However, higher dipole-bound states have not been observed experimentally. In the current work, we study the deprotonated 2-hydroxypyrimidine anion ($C_4H_3N_2O^-$ or 2-HOP, inset in Fig. 1), which may have more than one excited DBS because its neutral

* Corresponding author.
E-mail address: Lai-Sheng_Wang@brown.edu (L.-S. Wang).
[1] These authors contributed to the work equally.

http://dx.doi.org/10.1016/j.jms.2016.10.021
0022-2852/

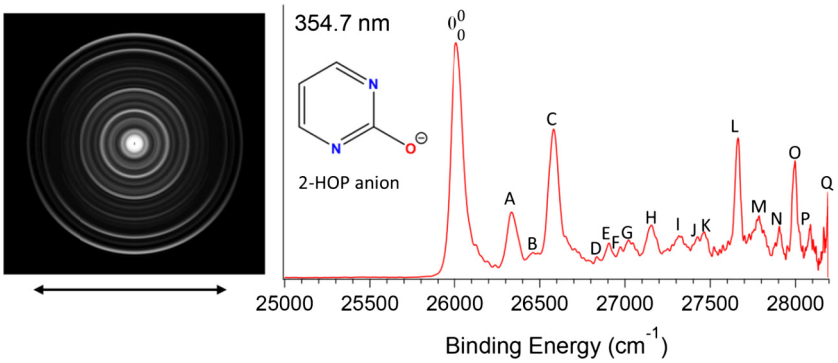

Fig. 1. Non-resonant photoelectron image and spectrum of $C_4H_3N_2O^-$ at 354.7 nm. The double arrow below the image indicates the directions of the laser polarization. The inset shows the structure of the deprotonated 2-hydroxypyrimidine (2-HOP) anion.

radical possesses a large dipole moment (estimated to be ~6.2 D). We have observed twenty resonant peaks in the photodetachment spectrum due to vibrational levels of the excited DBS, three of which are below the detachment threshold. Resonant PE images have been obtained via the seventeen above-threshold vibrational peaks, yielding highly non-Franck-Condon PE spectra. However, no evidence of an electronically excited second DBS below the detachment threshold is observed. The electron affinity of the $C_4H_3N_2O^{\cdot}$ radical or the detachment threshold of the $C_4H_3N_2O^-$ anion is measured accurately to be 26,010 ± 5 cm^{-1}. The binding energy of the ground vibrational level of the DBS relative to the detachment threshold is measured to be 598 ± 5 cm^{-1}.

2. Experimental methods

The experiment was carried out on our third-generation electrospray-PES apparatus [40], which consists of an electrospray ionization (ESI) source [41], a cryogenically-cooled Paul trap [42], a time-of-flight (TOF) mass spectrometer, and a high-resolution velocity-map imaging system [43]. Briefly, the $C_4H_3N_2O^-$ anions were produced via electrospray of a 1 mM solution of 2-hydroxypyrimidine dissolved in a mixed CH_3OH/H_2O (9/1 in volume) solvent at pH ~ 10. Two radio-frequency (RF) quadrupole and one RF octopole ion guides directed the anions from the ESI source into a cryogenically-cooled Paul trap operated at 4.5 K. The stored anions were cooled via collisions with 1 mTorr He/H_2 (4/1 in volume) buffer gas [42] and pulsed out at a 10 Hz repetition rate. The desired anions were selected by a mass gate, following mass analyses by the TOF mass spectrometer. Both a Nd:YAG laser (354.7 nm or 3.496 eV) and a dye laser were used for photodetachment. Photoelectrons were projected onto a pair of 75-mm diameter micro-channel plates coupled to a phosphor screen and finally captured by a charge-coupled device camera. The recorded PE images were inverse-Abel transformed and reconstructed using the pBasex [44] and BASEX [45] programs. The PE spectra were calibrated with the known spectra of Au^- at different photon energies. The kinetic energy (KE) resolution achieved was 3.8 cm^{-1} for 55 cm^{-1} KE electrons and about 1.5% (ΔKE/KE) for KE above 1 eV.

3. Results

3.1. The non-resonant photoelectron image and spectrum at 354.7 nm

Fig. 1 shows the non-resonant PE image and spectrum of $C_4H_3N_2O^-$ at 354.7 nm, representing detachment transitions from the vibrational ground state of the anion to the vibrational levels of the electronic ground state of the $C_4H_3N_2O^{\cdot}$ radical. Because of the complete elimination of vibrational hot bands, the first intense peak around ~26,000 cm^{-1} should correspond to the 0–0 transition. The higher binding energy peaks labeled from A to Q denote transitions to different excited vibrational levels of the neutral radical. The photoelectron angular distribution (PAD) of the intense 0–0 peak has $s + d$ character with an anisotropy (β) of −1, indicating that the highest occupied molecular orbital of the anion is a p-type orbital. The electron binding energies of all the observed vibrational peaks, their shifts from the first peak and assignments are summarized in Table 1, where the more accurate values are from the resonant PE images to be presented below.

3.2. Photodetachment spectroscopy

To search for the DBS, we measured the photodetachment spectrum by monitoring the total electron yield as a function of the dye laser wavelength near the detachment threshold [46], as shown in Fig. 2. The scanning step used was 0.03 nm and each step was averaged for 700 laser shots. The arrow at 26,010 cm^{-1} represents the detachment threshold, which is measured more accurately from the resonant PE spectrum in Fig. 3(a) (see below). The overall baseline above threshold represents the cross section of direct non-resonant detachment processes. Most prominently, seventeen sharp peaks are observed and labeled as 1–17 above the detachment threshold. These peaks indicate autodetachment from vibrational levels of the anticipated excited DBS of $C_4H_3N_2O^-$.

Below threshold, three weaker peaks, labeled as 0, α and β are observed due to resonant two-photon detachment. The peak 0 at 25,412 cm^{-1} represents the ground vibrational level of the DBS, corresponding to the outmost ring of the inset PE image. The PAD of the resonant two-photon detachment image gives an anisotropy parameter of 1.6, i.e., of p-wave character, which is very different from the $s + d$ character shown in the non-resonant detachment features in Fig. 1. The p-wave character of the resonant two-photon PE image indicates that the intermediate state is an s-type orbital, consistent with the nature of the DBS, as was also observed previously [28,31,32,35]. The binding energy of the DBS, referring as the energy difference between the neutral ground state and the vibrational ground state of the DBS, is determined to be 598 ± 5 cm^{-1}. The weak peaks α and β correspond to low-frequency vibrational levels of the DBS below the detachment threshold and can only be accessed via two-photon processes.

The top scale in Fig. 2 is relative to the vibrational ground state of the DBS. The observed photon energies, shifts from the ground vibrational level of the DBS, and assignments of the observed vibrational resonances are given in Table 2. The assignments of peaks 1–17 are all based on the resonant autodetachment PE

Table 1
Observed vibrational peaks and their binding energies (BE) from PE spectra of $C_4H_3N_2O^-$. The shifts from the 0–0 transition and assignments are also given. The peaks labeled 0_0^0 and A–Q correspond to those observed in the non-resonant PE spectrum in Fig. 1. Peaks a–d are from resonant spectra in Figs. 3 and 4. Numbers in parentheses indicate the experimental uncertainties. The binding energies of peaks 0_0^0 and A–C are derived from resonant PE spectra, which give more accurate values. The assignments for peaks J–Q are tentative (see text).

Peaks	BE (cm^{-1})	Shift (cm^{-1})	Assignment
0_0^0	26,010(5)	0	Neutral ground state
A	26,330(5)	320	2^1
B	26,463(5)	453	3^1
C	26,585(5)	575	5^1
D	26,835(30)	825	1^17^1
E	26,906(30)	896	1^35^1
F	26,973(30)	963	11^1
G	27,022(30)	1012	13^1
H	27,155(30)	1145	5^2
I	27,318(30)	1308	5^17^1
J	27,426(30)	1416	(5^19^1)
K	27,465(30)	1455	(2^15^2)
L	27,663(20)	1653	(2^117^1)
M	27,778(20)	1768	(2^119^1)
N	27,905(20)	1895	(2^121^1)
O	27,994(20)	1984	(5^29^1)
P	28,084(20)	2074	(2^219^1)
Q	28,190(20)	2180	(5^121^1)
a	26,113(5)	103	1^1
b	26,215(5)	205	1^2
c	26,559(5)	549	4^1
d	26,660(5)	650	6^1

spectra in Figs. 3 and 4 and the calculated vibrational frequencies shown in Table 3.

3.3. Resonant photoelectron images and spectra

By tuning the detachment laser to the above-threshold vibrational peaks, we obtained seventeen high-resolution resonantly enhanced PE images and spectra, as shown in Figs. 3 and 4. Two detachment channels contribute to these spectra: the regular non-resonant photodetachment represented by the baseline above the detachment threshold in Fig. 2 and the resonantly-enhanced vibrational autodetachment via the DBS. The four spectra shown in Fig. 3 contain autodetachment involving a single vibrational mode of the DBS, while those given in Fig. 4 correspond to excitations to vibrational levels of combinational modes of the DBS. Due to the mode selectivity and the $\Delta v = -1$ propensity rule in the autodetachment process [28–35], certain vibrational levels are enhanced in the resonant PE spectra, resulting in completely non-Franck-Condon distributions relative to the non-resonant PE spectrum in Fig. 1. The assignments (in bold face) in Fig. 4 indicate the major enhanced vibrational peaks. Numerous Franck-Condon inactive or unresolved peaks in Fig. 1 are observed in the resonant spectra, labeled as *a–d*. The binding energies, shifts from the 0_0^0 peak and assignments of peaks *a–d* are given in Table 1.

4. Discussion

4.1. The non-resonant photoelectron spectrum

The vibrational peaks shown in the non-resonant PE spectrum in Fig. 1 are governed by the Franck-Condon principle, and only symmetry-allowed modes with significant Franck-Condon factors can be observed. To guide the assignments of these peaks, we carried out density functional theory calculations at the B3LYP/6-311++G(d, p) level for the vibrational frequencies of the corresponding neutral radical ($C_4H_3N_2O^{\cdot}$). The calculated vibrational frequencies (unscaled) for the twenty-four normal modes are given in Table 3 in increasing order of frequencies. As shown previously, the unscaled B3LYP frequencies are very helpful in the spectral assignments [31–35] and are in general in good agreement with the observed frequencies for most vibrational modes.

Because both the anion and the neutral radical of 2-HOP have C_{2v} symmetry, only modes containing A_1 symmetry are allowed. By comparing the experimental shifts with the theoretical frequencies, we can readily assign peaks C-I to the 5^1, 1^17^1, 1^35^1, 11^1, 13^1, 5^2, and 5^17^1 vibrational levels, respectively, which are also confirmed by the photodetachment spectrum and the resonant PE spectra to be discussed below. The ν_5 mode, corresponding to the in-plane deformation of the whole ring, is observed to be the main Franck-Condon-active mode. Peaks A and B with shifts of 320 cm^{-1} and 453 cm^{-1} agree well with the computed frequencies of the ν_2 (A_2, 316 cm^{-1}) and ν_3 (B_1, 468 cm^{-1}) modes (Table 3).

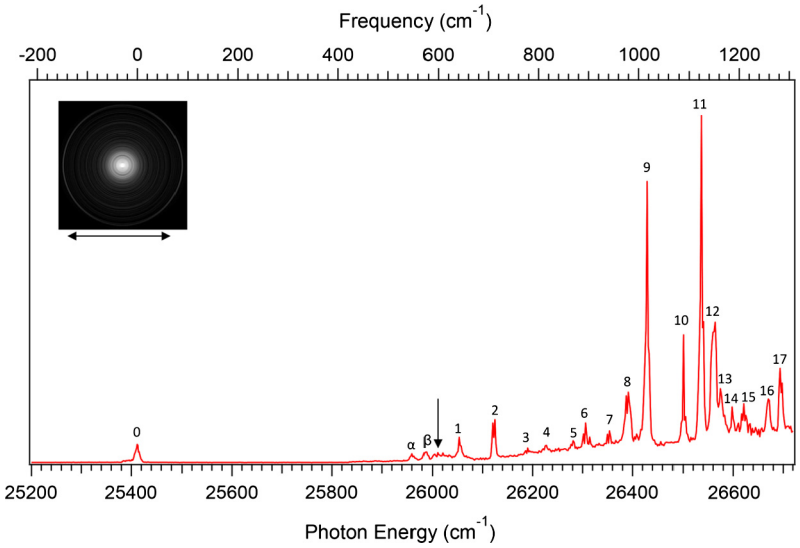

Fig. 2. The photodetachment spectrum of $C_4H_3N_2O^-$ by measuring the total electron yield as a function of photon energy near the detachment threshold. The arrow indicates the detachment threshold. The above threshold peaks labeled as 1–17 are due to autodetachment from vibrational levels of the DBS of $C_4H_3N_2O^-$. The below-threshold peaks 0, α and β are due to single color resonant two-photon detachment. The inset PE image represents the resonant two-photon detachment spectrum at peak 0. The double arrow below the image indicates the directions of the laser polarization.

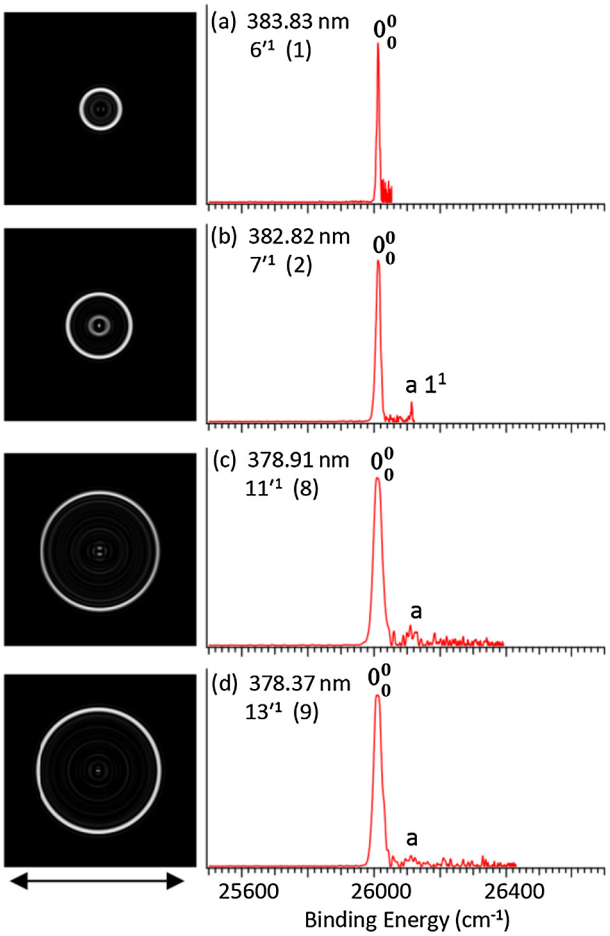

Fig. 3. Resonant PE images and spectra of $C_4H_3N_2O^-$ at four different detachment wavelengths, corresponding to autodetachments involving single vibrational modes. The peak number (in parentheses) corresponds to that in Fig. 2 and the vibrational levels of the DBS are given. The double arrow below the images indicates the directions of the laser polarization.

These two modes are due to out-of-plane ring-bending and are symmetry-forbidden. Their activities may be due to strong vibronic coupling effects. There is considerable intensity for the ν_2 mode, which may also suggest a slight out-of-plane distortion in the neutral 2-HOP radical. The higher binding energy peaks from J to Q in Fig. 1 are all tentatively assigned to combinational levels of the two Franck-Condon-active modes (ν_2 and ν_5) with other modes on the basis of the theoretical frequencies.

4.2. The photodetachment spectrum

The neutral 2-HOP radical ($C_4H_3N_2O^{\cdot}$) has a calculated dipole moment of ~6.2 D, larger than the minimum value of 4.5 D predicted by Garrett [38,39] for a second bound DBS. The photodetachment spectrum in Fig. 2 shows three peaks, 0, α and β, below threshold. In addition to the ground vibrational level (peak 0) of the DBS, the peaks α and β can be assigned to the ν_4 and ν_5 fundamental vibrational modes (Table 2) based on the computed frequencies in Table 3. Thus, no evidence is observed for a second bound electronically excited DBS.

The seventeen above-threshold peaks represent optical excitations to the vibrational levels of the DBS followed by autodetachment and they display asymmetric Fano line shapes [47,48] as a result of the interference between the non-resonant detachment and autodetachment channels. The Fano line shape is seen more clearly for the strong and well-resolved peak 9. Inasmuch as the excess electron in the DBS is weakly bound and has little effect to the neutral core, the vibrational frequencies of the DBS of the anion are the same as the corresponding neutral radical within our experimental uncertainty [28,31–35,46]. This observation means that the observed vibrational frequencies in the photodetachment spectrum in Fig. 2 can be combined with the non-resonant and resonant PE spectra to yield vibrational information for the neutral radical [28,31–35,46]. Thus, even though we use a prime to designate the vibrational levels of the DBS, the vibrational frequencies should be the same from the PE spectra for the same mode. For example, the vibrational frequency for the ν'_5 mode (574 cm^{-1}) of the DBS in Table 2 is the same as the ν_5 mode of the neutral radical measured from the PE spectra given in Table 1 (575 cm^{-1}). The experimental frequencies shown in Table 3 are obtained from both PE spectra and the photodetachment spectrum. In general, the photodetachment spectrum gives more accurate vibrational frequencies, mainly limited by the rotational broadening. The assignments of the photodetachment peaks given in Table 2 are accomplished by the resonant PE spectra presented in Figs. 3 and 4 below, as well as by comparison with the calculated frequencies.

Table 2
The observed peaks, photon energies, shifts from peak 0 and assignments of the vibrational resonances in Fig. 2. Numbers in parentheses indicate the experimental uncertainties.

Peak	Photon energy (cm^{-1})	Shift (cm^{-1})	Assignment
0	25,412(5)	0	Ground DBS
α	25,960(5)	548	$4'^1$
β	25,986(5)	574	$5'^1$
1	26,053(5)	641	$6'^1$
2	26,122(5)	710	$7'^1$
3	26,199(5)	787	$1'^2 5'^1$
4	26,225(5)	813	$1'^1 7'^1$
5	26,278(5)	866	$1'^3 4'^1$
6	26,305(5)	893	$1'^3 5'^1$
7	26,354(5)	942	$2'^1 6'^1$
8	26,391(5)	979	$11'^1$
9	26,429(5)	1017	$13'^1$
10	26,501(5)	1089	$1'^3 2'^1 3'^1$
11	26,537(5)	1125	$2'^1 8'^1$
12	26,560(5)	1148	$1'^1 3'^1 5'^1$
13	26,572(5)	1160	$3'^1 7'^1$
14	26,599(5)	1187	$4'^1 6'^1$
15	26,621(5)	1209	$5'^1 6'^1$
16	26,671(5)	1259	$4'^1 7'^1$
17	26,694(5)	1282	$5'^1 7'^1$

4.3. Autodetachments involving single-mode vibrational levels of the DBS

As reported previously [28,31–35], autodetachment from DBS's to final neutral states follows the $\Delta v = -1$ propensity rule, i.e., the nth vibrational level of a given mode (v'^n_x) of the DBS autodetaches to the $(n-1)$th level of the corresponding neutral mode (v_x^{n-1}). This propensity of autodetachment, stemmed from the fact that the structure of the DBS is similar to that of the neutral final state [29,30], gives rise to the mode selectivity and highly non-Franck-Condon resonant PE spectra. Fig. 3 shows that the 0_0^0 peak is greatly enhanced in each case (much stronger signals), indicating autodetachment from the fundamental vibrational level (v'^1_x) of the DBS. The PAD of the 0_0^0 peak is isotropic in each case, different from the $s+d$ character shown in the non-resonant spectrum in Fig. 1. The photon energies shown in Fig. 3 correspond to resonant excitations to the $6'^1$, $7'^1$, $11'^1$ and $13'^1$ levels of the DBS, respectively.

A weak peak *a* is also observed in Fig. 3b–d. As given in Table 1, the shift of peak *a* relative to the 0_0^0 peak is 103 cm^{-1}, which

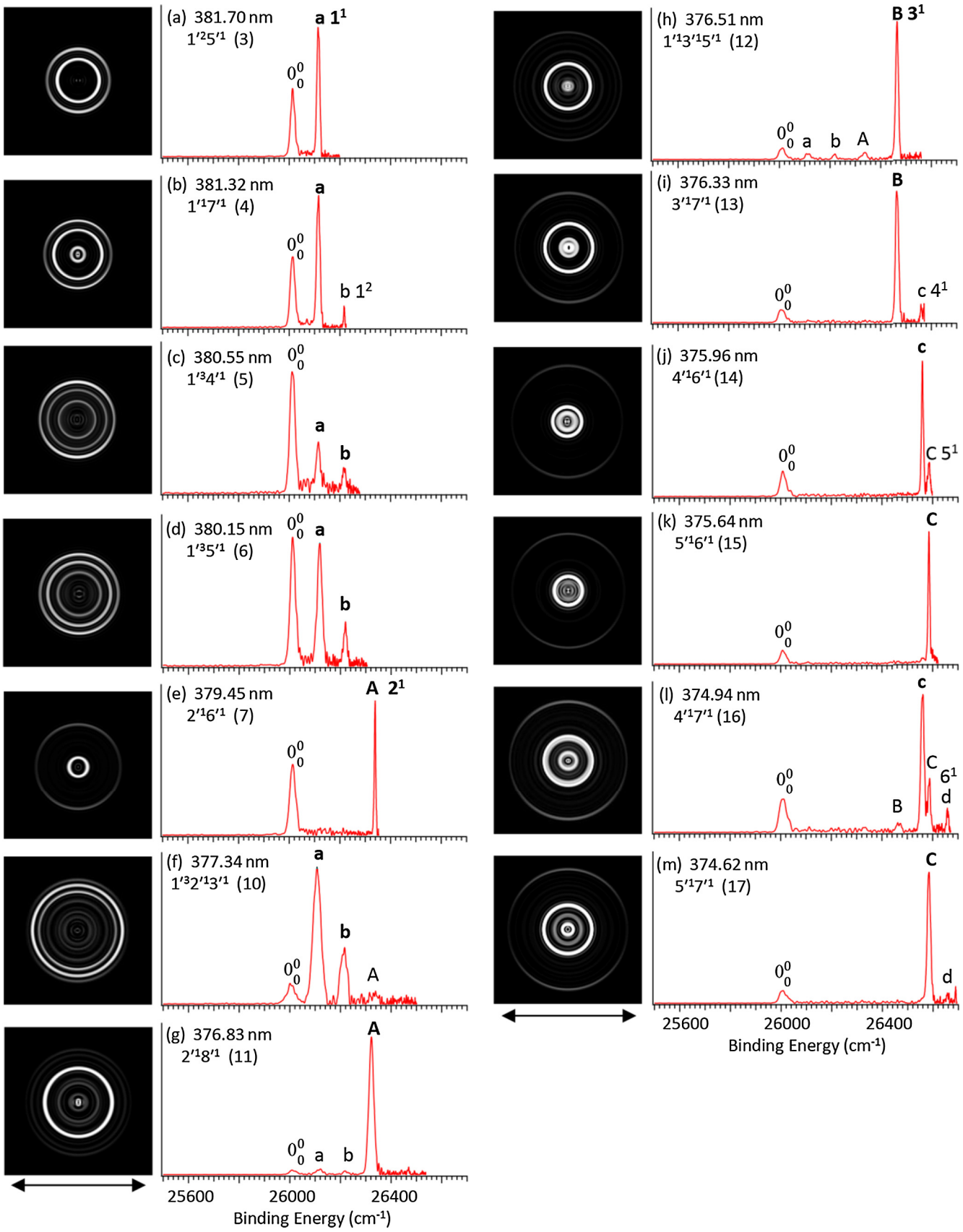

Fig. 4. Resonant PE images and spectra of $C_4H_3N_2O^-$ at thirteen different detachment wavelengths, corresponding to excitations to combinational vibrational levels of the DBS. The peak number (in parentheses) corresponds to that in Fig. 2 and the vibrational levels of the DBS are given. The double arrows below the images indicates the directions of the laser polarization. The labels in bold face mark the enhanced final neutral vibrational levels.

Table 3
The harmonic frequencies for $C_4H_3N_2O^{\cdot}$ calculated using density functional theory at the B3LYP/6-311++G(d, p) level. The nine experimental frequencies, including six from resonant peaks in Fig. 2, are given to compare.

Mode	Symmetry	Cal. Freq. (cm^{-1})	Exp. Freq. (cm^{-1})	Peak
ν_1	B1	119	103(5)	
ν_2	A2	316	320(5)	
ν_3	B1	468	454(5)	
ν_4	B2	516	548(5)	α
ν_5	A1	584	574(5)	β
ν_6	B2	627	641(5)	1
ν_7	B1	742	710(5)	2
ν_8	A1	799		
ν_9	B1	837		
ν_{10}	A2	962		
ν_{11}	A1	992	979(5)	8
ν_{12}	B1	992		
ν_{13}	A1	1040	1017(5)	9
ν_{14}	B2	1090		
ν_{15}	B2	1166		
ν_{16}	B2	1299		
ν_{17}	A1	1322		
ν_{18}	B2	1425		
ν_{19}	A1	1433		
ν_{20}	B2	1511		
ν_{21}	A1	1597		
ν_{22}	A1	3141		
ν_{23}	B2	3142		
ν_{24}	A1	3204		

corresponds to the fundamental vibrational frequency of the lowest frequency mode $\nu_1(B_1)$ with a computed frequency of 119 cm^{-1} (Table 3). The ν_1 mode is an out-of-plane bending mode and is symmetry-forbidden in the non-resonant spectrum. Its appearance in Fig. 3b–d is most likely due to the intramolecular electron rescattering effect, as discussed recently in the resonant PE spectra of the deprotonated uracil anion [33].

4.4. Autodetachment from combinational vibrational levels of the DBS

For the excitation to a combinational vibrational level ($\nu'_x{}^m\nu'_y{}^n\ldots$) of the DBS, the final neutral level from autodetachment can be either $\nu_x^{m-1}\nu_y^n\ldots$ or $\nu_x^m\nu_y^{n-1}\ldots$, based on the $\Delta\nu = -1$ propensity rule and mode-selectivity. The PE spectra in Fig. 4 are all due to autodetachment from combinational vibrational levels of the DBS. In all these spectra, the 0_0^0 peak is from direct photodetachment, as confirmed by its $s + d$ PAD; all the higher vibrational levels are enhanced due to autodetachment, as can also be seen from their isotropic PADs.

A number of the spectra (Fig. 4a–d and f) show strong intensities for two low binding energy peaks, labeled as *a* and *b*, which are due to the fundamental (103 cm^{-1}) and overtone (205 cm^{-1}) of the lowest vibrational mode (ν_1) of the 2-HOP radical (Table 1). This is a bending mode with negligible Franck-Condon factors in the non-resonant PE spectrum (Fig. 1). The autodetaching vibrational levels corresponding to these spectra must involve combinational levels of the ν_1 mode with other high frequency modes. All the vibrational levels of the DBS are given in each spectrum in Fig. 4, as well as the peak numbers of the corresponding resonant peaks in the photodetachment spectrum. Interestingly, in all of these cases involving the ν_1 mode the $\Delta\nu = -1$ propensity rule is broken. For example, Fig. 4a involves resonant excitation to the $1'^2 5'^1$ combinational level of the DBS. To reach the 1^1 final state, one quantum of the ν'_1 mode and one quantum of the ν'_5 mode must be coupled to the outgoing electron during the autodetachment. In the case of Fig. 4d ($1'^3 5'^1$), two quanta of the ν'_1 mode and one quantum of the ν'_5 mode are required to reach the 1^1 final state. These observations suggest that the ν'_1 mode must be highly anharmonic. The photodetachment spectrum in Fig. 2 shows that the resonant enhancement to these vibrational levels of the DBS is quite weak, even though the corresponding resonant PE spectra are dramatically different. The current observation is consistent with our previous studies [28,31–35], which demonstrate that resonant PE spectra via the DBS are quite powerful in providing vibrational information than traditional PES.

The assignments of the remaining spectra in Fig. 4 are fairly straightforward. In all these cases except Fig. 4h, a combinational vibrational level between a low frequency and high frequency mode is involved. Because of the high binding energy of the DBS (598 cm^{-1}), only the higher frequency mode in these cases has enough vibrational energy to couple to the DBS electron to cause autodetachment. Hence, in all these spectra, only one vibrational final state due to the lower frequency mode is observed to be enhanced. The observation of peaks *a* and *b* corresponding to excitation of the ν_1 mode in Fig. 4g is surprising, which is most likely due to the intramolecular rescattering effects between the outgoing DBS electron and the neutral core, as observed more prominently in the deprotonated uracil case recently [33]. The spectrum in Fig. 4h needs some comment. The DBS level corresponding to peak 12 in Fig. 2 is assigned to a combinational level of $1'^1 3'^1 5'^1$. However, the strong enhancement of the 3^1 final state suggests that there may be an overlap between peaks 12 and 13, as they are very closely spaced (see Fig. 2). The discernible intensity of peaks *a* and *b* in Fig. 4h may be also due to the intramolecular rescattering effects, as invoked for Fig. 4g.

The related vibrational levels of the DBS and the 2-HOP radical final states, the autodetachment processes, and the associated energetics are given in Fig. 5.

5. Conclusions

In conclusion, we report a high resolution photoelectron imaging and photodetachment study of cold deprotonated 2-hydroxypyrimidine anion ($C_4H_3N_2O^-$). A dipole-bound ground state is observed with a binding energy of 598 ± 5 cm^{-1} due to the large dipole moment of the $C_4H_3N_2O^{\cdot}$ radical. However, no evidence is observed for a second electronically bound dipole-bound state below the detachment threshold, despite the large dipole

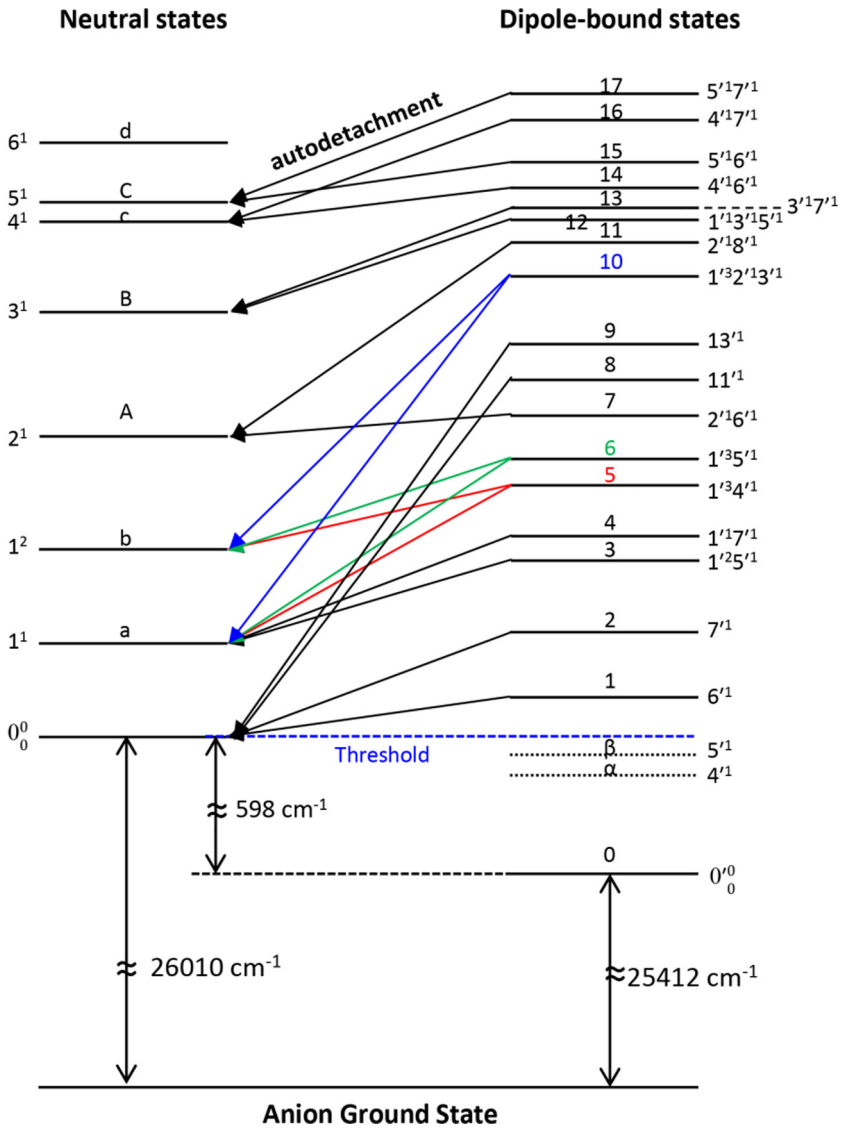

Fig. 5. Schematic energy level diagram for autodetachment from the vibrational levels of the DBS to the neutral final states. The detachment threshold (blue dash line) of the $C_4H_3N_2O^-$ and the binding energy of the DBS are shown. Autodetachment processes are indicated by the arrows, whereas multiple autodetachment channels from a given DBS level are given in colors. The vibrational levels of the DBS, labeled as 0–17, α, β, correspond to peaks in Fig. 2. And the assignments for DBS and neutral states are all given in Tables 1 and 2. (For interpretation of the references to color in this figure legend, the reader is referred to the web version of this article.)

moment of the neutral core. Twenty vibrational levels of the DBS are observed as resonant peaks in the photodetachment spectrum. Seventeen resonant photoelectron spectra are obtained by tuning the detachment laser to each of the seventeen above-threshold vibrational resonances. These resonant PE spectra are highly non-Franck-Condon due to the vibrational propensity of the autodetachment processes. In total, nine fundamental vibrational frequencies are obtained, including the six symmetry-forbidden modes. The current study provides another example showing that resonant PES via the dipole-bound states of cold anions is a powerful approach to obtain vibrational information for dipolar radicals.

Acknowledgement

We would like to thank Dr. Hong-Tao Liu and Dr. Chuan-Gang Ning for experimental assistance and valuable discussions. This work was supported by the National Science Foundation.

References

[1] R.N. Compton, N.I. Hammer, Advances in Gas-Phase Ion Chemistry, in: N. Adams, I. Babcock (Eds.), vol. 4, Elsevier Science, New York, 2001, pp. 257–291.
[2] K.D. Jordan, F. Wang, Annu. Rev. Phys. Chem. 54 (2003) 367–396.
[3] E. Fermi, E. Teller, Phys. Rev. 72 (1947) 399–408.
[4] O.H. Crawford, Mol. Phys. 20 (1971) 585–591.
[5] W.R. Garrett, Phys. Rev. A 3 (1971) 961–972.
[6] O.H. Crawford, W.R. Garrett, J. Chem. Phys. 66 (1977) 4968–4970.
[7] C. Desfrançois, H. Abdoul-Carime, N. Khelifa, J.P. Schermann, Phys. Rev. Lett. 73 (1994) 2436–2439.
[8] C. Desfrançois, H. Abdoul-Carime, J.P. Scherman, Int. J. Mod. Phys. B 10 (1996) 1339.
[9] N.I. Hammer, K. Diri, K.D. Jordan, C. Desfrançois, R.N. Compton, J. Chem. Phys. 119 (2003) 3650–3660.
[10] L. Suess, Y. Liu, R. Parthasarathy, F.B. Dunning, J. Chem. Phys. 119 (2003) 12890–12894.
[11] S. Xu, W. Zheng, D. Radisic, K.H. Bowen Jr., J. Chem. Phys. 122 (2005) 091103.
[12] J.H. Hendricks, S.A. Lyapustina, H.L. de Clercq, J.T. Snodgrass, K.H. Bowen, J. Chem. Phys. 104 (1996) 7788–7791.
[13] A.M. Buytendyk, A.M. Buonaugurio, S.J. Xu, J.M. Nilles, K.H. Bowen, N. Kirnosov, L. Adamowicz, J. Chem. Phys. 145 (2016) 024301.
[14] A.H. Zimmerman, J.I. Brauman, J. Chem. Phys. 66 (1977) 5823–5825.
[15] R.D. Mead, K.R. Lykke, W.C. Lineberger, J. Marks, J.I. Brauman, J. Chem. Phys. 81 (1984) 4883–4892.

[16] K.R. Lykke, R.D. Mead, W.C. Lineberger, Phys. Rev. Lett. 52 (1984) 2221–2224.
[17] K. Yokoyama, G.W. Leach, J.B. Kim, W.C. Lineberger, J. Chem. Phys. 105 (1996) 10696–10705.
[18] K. Yokoyama, G.W. Leach, J.B. Kim, W.C. Lineberger, A.I. Boldyrev, M. Gutowski, J. Chem. Phys. 105 (1996) 10706–10718.
[19] R.N. Compton, J.H.S. Carman, C. Desfrancois, H. Abdoul-Carime, J.P. Schermann, J.H. Hendricks, S.A. Lyapustina, K.H. Bowen, J. Chem. Phys. 105 (1996) 3472–3478.
[20] J.H. Hendricks, S.A. Lyapustina, H.L. de Clercq, K.H. Bowen, J. Chem. Phys. 108 (1998) 8–11.
[21] T. Sommerfeld, Phys. Chem. Chem. Phys. 4 (2002) 2511–2516.
[22] C.E.H. Dessent, C.G. Bailey, M.A. Johnson, J. Chem. Phys. 102 (1995) 6335–6338.
[23] C.E.H. Dessent, C.G. Bailey, M.A. Johnson, J. Chem. Phys. 103 (1995) 2006–2015.
[24] M.A. Yandell, S.B. King, D.M. Neumark, J. Chem. Phys. 140 (2014) 184317.
[25] P.J. Sarre, Mon. Not. R. Astron. Soc. 313 (2000) 14–16.
[26] F. Güthe, M. Tulej, M.V. Pachkov, J.P. Maier, Astrophys. J. 555 (2001) 466–471.
[27] R.C. Fortenberry, T.D. Crawford, T.J. Lee, Astrophys. J. 762 (2013) 121.
[28] H.T. Liu, C.G. Ning, D.L. Huang, P.D. Dau, L.S. Wang, Angew. Chem. Int. Ed. 52 (2013) 8976.
[29] R.S. Berry, J. Chem. Phys. 45 (1966) 1228.
[30] J. Simons, J. Am. Chem. Soc. 103 (1981) 3971.
[31] D.L. Huang, H.T. Liu, C.G. Ning, L.S. Wang, J. Chem. Phys. 142 (2015) 124309.
[32] D.L. Huang, H.T. Liu, C.G. Ning, G.Z. Zhu, L.S. Wang, Chem. Sci. 6 (2015) 3129.
[33] D.L. Huang, H.T. Liu, C.G. Ning, P.D. Dau, L.S. Wang, Chem. Phys. (2016), http://dx.doi.org/10.1016/j.chemphys.2016.06.003.
[34] D.L. Huang, G.Z. Zhu, L.S. Wang, J. Chem. Phys. 142 (2015) 091103.
[35] D.L. Huang, H.T. Liu, C.G. Ning, L.S. Wang, J. Phys. Chem. Lett. 6 (2015) 2153.
[36] R.F. Wallis, R. Herman, H.W. Milnes, J. Mol. Spectrosc. 4 (1960) 51.
[37] O.H. Crawford, Proc. Phys. Soc. 91 (1967) 279–284.
[38] W.R. Garrett, J. Chem. Phys. 73 (1980) 5721.
[39] W.R. Garrett, J. Chem. Phys. 77 (1982) 3666.
[40] L.S. Wang, J. Chem. Phys. 143 (2015) 040901.
[41] L.S. Wang, C.F. Ding, X.B. Wang, S.E. Barlow, Rev. Sci. Instrum. 70 (1999) 1957.
[42] X.B. Wang, L.S. Wang, Rev. Sci. Instrum. 79 (2008) 073108.
[43] I. León, Z. Yang, H.T. Liu, L.S. Wang, Rev. Sci. Instrum. 85 (2014) 083196.
[44] G.A. Garcia, L. Nahon, I. Powis, Rev. Sci. Instrum. 75 (2004) 4989.
[45] V. Dribinski, A. Ossadtchi, V.A. Mandelshtam, H. Reisler, Rev. Sci. Instrum. 73 (2002) 2634.
[46] H.T. Liu, C.G. Ning, D.L. Huang, L.S. Wang, Angew. Chem. Int. Ed. 53 (2014) 2464–2468.
[47] U. Fano, Phys. Rev. 124 (1961) 1866.
[48] S.T. Edwards, M.A. Johnson, J.C. Tully, J. Chem. Phys. 136 (2012) 154305.